drones

MDPI

Article

Robust Consensus Tracking Control for Multi-Unmanned-Aerial-Vehicle (UAV) System Subjected to Measurement Noise and External Disturbance

Zhiyuan Zheng [1], Shiji Tong [2], Erquan Wang [3], Yang Zhu [3] and Jinliang Shao [1,*]

[1] School of Automation Engineering, University of Electronic Science and Technology of China, Chengdu 611731, China; z.zheng@std.uestc.edu.cn
[2] School of Aeronautics and Astronautics, University of Electronic Science and Technology of China, Chengdu 611731, China; shijitong@std.uestc.edu.cn
[3] School of Information Science and Technology, Southwest Jiaotong University, Chengdu 611756, China; wangerquan@my.swjtu.edu.cn (E.W.); zhuyang@swjtu.edu.cn (Y.Z.)
* Correspondence: jinliangshao@uestc.edu.cn

Abstract: In practice, the consensus performance of a multi-UAV system can degrade significantly due to the presence of measurement noise and disturbances. However, simultaneously rejecting the noise and disturbances to achieve high-precision consensus tracking control is rather challenging. In this paper, to address this issue, we propose a novel distributed consensus tracking control framework consisting of a distributed observer and a local dual-estimator-based tracking controller. Each UAV's distributed observer estimates the leader's states and generates the local reference, functioning even under a switching communication topology. In the local tracking controller design, we reveal that classic uncertainty and disturbance estimator (UDE)-based control can magnify the noise. By combining the measurement error estimator (MEE) with UDE, a local robust tracking controller is designed to reject noise and disturbances simultaneously. The parameter tuning of MEE and UDE is unified into a single parameter, and the monotonic relationship between this parameter and system performance is revealed by the singular perturbation theorem. Finally, the validity of the proposed control framework is verified by both simulation and comparative real-world experiments.

Keywords: multi-UAV systems; consensus tracking control; distributed control; measurement noise and disturbance rejection

check for updates

Academic Editor: Oleg Yakimenko

Received: 26 November 2024
Revised: 8 January 2025
Accepted: 14 January 2025
Published: 16 January 2025

Citation: Zheng, Z.; Tong, S.; Wang, E.; Zhu, Y.; Shao, J. Robust Consensus Tracking Control for Multi-Unmanned-Aerial-Vehicle (UAV) System Subjected to Measurement Noise and External Disturbance. *Drones* **2025**, *9*, 61. https://doi.org/10.3390/drones9010061

Copyright: © 2025 by the authors. Licensee MDPI, Basel, Switzerland. This article is an open access article distributed under the terms and conditions of the Creative Commons Attribution (CC BY) license (https://creativecommons.org/licenses/by/4.0/).

1. Introduction

Multi-unmanned-aerial-vehicle (UAV) systems have attracted significant attention in recent years due to their inherent advantages, including scalability, flexibility, distributed decision-making, and robustness [1–3]. These attributes make multi-UAV systems widely applied in various practical applications such as aerial transportation [4–6], disaster data collection [7,8], area search [9,10], etc.

Consensus control is a fundamental control problem in the field of UAV swarms and has received significant attention from researchers, which means the UAVs in a group reach an agreement via information interaction. The work [11] proposes a model-free distributed consensus tracking protocol that does not require the eigenvalues of the graph matrix via the adaptive observer and system identification process. In [12], the distributed adaptive protocol is proposed to achieve bipartite consensus tracking for systems without knowing the leader's input. Furthermore, to reject the disturbance and improve the

system's robustness, various consensus methods have been explored. In the work [13], the authors propose a robust decentralized protocol to achieve predefined-time consensus convergence for multi-UAV systems under bounded external disturbances and switching communication topology. A fixed-time controller is proposed in [14] based on the adding-a-power-integrator method to achieve consensus tracking in finite time for multi-UAV systems with matched and mismatched disturbances. The work [15] proposes a hierarchical distributed control framework consisting of a reference signal generator and a tracking controller, which can deal with representative issues for multi-UAV systems like mismatched disturbance and communication issues.

However, the literature above has a practical limitation: it ignores the measurement noise in each UAV's state. Since the consensus control of multi-UAV systems heavily relies on the information interaction among UAVs, the inaccurate information of a single UAV may mislead the action of the entire system, thereby degrading the system performance or even leading to instability [16]. In the work [17], the authors propose a distributed Kalman-consensus filter to achieve the cooperative estimation of a mobile target with noise. The work [18] combines the model predictive control with the Kalman-consensus filter and a fixed-time disturbance observer to achieve the formation control of multi-UAV systems. Considering the measurement noise in a communication network, the work [19] supposes that followers can only measure the relative position of their neighbors in a noisy environment and develops a neighbor-based tracking protocol based on a velocity decomposition technique to achieve leader–follower tracking control. Additive noises are considered in [20], where the authors propose the concept of pure group and hybrid group consensus and reveal that the relationship between the two group influences the attenuation rate and the control gain matrix. In the work [21], the authors consider both additive and multiplicative measurement noise and develop a stochastic weak and strong consensus condition under fixed and time-varying topologies. In the scenario where noise and disturbances both exist, the authors of [22] propose a scale-free collaborative protocol that does not need communication topology information or the number of UAVs to achieve output synchronizations for multi-UAV systems with known frequency disturbance and measurement noise. Moreover, the work [23] presents a distributed observer-based H_∞ consensus control that transforms the consensus problem into a corresponding linear system stabilization problem for multi-UAV systems with measurement noise and disturbance.

Switching topologies should also be considered, as communication links and UAVs within the swarm may experience faults in practice. In the work [24], the authors consider the disturbance and measurement noise in $\mathcal{L}_2$ space and achieve distributed estimation under the switching topology. However, the consensus tracking problem has not been investigated. Achieving consensus under noise, disturbances, and switching topologies is challenging due to the strong coupling of these factors. The robust consensus control for multi-UAV systems with noise and disturbance under switch topologies is still to be investigated. Furthermore, the aforementioned methods have only been verified through numerical simulation, with no experimental results to support their effectiveness.

Motivated by the vision of achieving high-precision consensus tracking control for multi-UAV systems subjected to measurement noise and disturbance under the switching topology, we propose a dual-estimator-based distributed control framework in this paper. Specifically, a distributed observer is designed to generate the local reference for each follower UAV under the switching communication topology. To reject the measurement noise and disturbance, MEE and UDE are designed in a coupled manner in the frequency domain. The proposed methodology can be applied to a class of systems with a linear second-order form. By using the singular perturbation theorem, the monotonic relationship between the controller parameter and system performance is revealed. The proposed control framework

is verified using the quadrotor model by numerical simulation. Moreover, since the simulation cannot reflect the key properties of the sensors, we conduct real-world experiments on a reduced quadrotor platform and compare the proposed control framework with other robust controllers: the robust integral of the sign of the error (RISE) and the extended state observer (ESO). The contributions of this paper can be summarized as follows.

1. To simultaneously reject the measurement noise and disturbances for multi-UAV systems, we propose a novel control framework that integrates a distributed observer and a local dual-estimator-based tracking controller. This hierarchical design manner decouples the noise and disturbance rejection control for each UAV from the leader's states and other UAVs.
2. To address the multi-parameter optimization issue in practice, we use a single parameter to unify the MEE and UDE parameter tuning. The qualitative relationship between this parameter and system control performance is revealed by the singular perturbation theorem. By monotonically reducing this parameter, the system control performance can be improved.
3. Comparative experiments are implemented to verify the feasibility and effectiveness of the proposed control methods with RISE and ESO.

The remainder of this paper is organized as follows. Section 2 gives the problem formulation and communication topology definition. The proposed distributed control framework containing the distributed observer and MEE+UDE is designed in Section 3. In Section 4, we discuss the analysis of the proposed control framework. Section 5 proposes the simulation study on the quadrotor model. Section 6 gives the experimental results. Section 7 is the conclusion of this paper.

2. Problem Formulation

In this paper, we will investigate the robust consensus tracking control of multi-UAV systems with measurement noise and disturbance in the double-integrator form:

$$\begin{aligned} \dot{\boldsymbol{x}}_i &= \boldsymbol{A}\boldsymbol{x}_i + \boldsymbol{B}(u_i + d_i), && (1)\\ \boldsymbol{y}_i &= \boldsymbol{C}\boldsymbol{x}_i + \boldsymbol{D}\omega_i, \quad i = 1, \ldots, N, && (2) \end{aligned}$$

where $\boldsymbol{x}_i = [x_{i1}, x_{i2}]^T \in \mathbb{R}^2$ are the UAV's position and velocity, $\boldsymbol{y}_i = [y_{i1}, y_{i2}]^T \in \mathbb{R}^2$ are the measured system output, $u_i \in \mathbb{R}$ denotes the system input, $d_i \in \mathbb{R}$ is the unknown external input disturbance, $\omega_i \in \mathbb{R}$ is the velocity measurement noise, and the coefficient matrices $\boldsymbol{A}, \boldsymbol{B}, \boldsymbol{C}, \boldsymbol{D}$ are given by

$$\begin{aligned} \boldsymbol{A} &= \begin{bmatrix} 0 & 1 \\ \alpha_1 & \alpha_2 \end{bmatrix}, \boldsymbol{B} = \begin{bmatrix} 0 \\ 1 \end{bmatrix}, \\ \boldsymbol{C} &= \begin{bmatrix} 1 & 0 \\ 0 & 1 \end{bmatrix}, \quad \boldsymbol{D} = \begin{bmatrix} 0 \\ 1 \end{bmatrix}, \end{aligned} \tag{3}$$

wherein α_1 and α_2 are the known constants. We assume that all UAVs have identical dynamics, and herein, we use the subscript "i" to represent the i-th UAV's states.

Assumption 1. *The derivatives of the measurement noise and input disturbance are bounded; i.e., there exist constants $\bar{\omega}$ and $\bar{d}$, such that $|\dot{\omega}(t)| \leq \bar{\omega}$, $|\dot{d}(t)| \leq \bar{d}$, $\forall t \geq 0$.*

Remark 1. *In Assumption 1, we consider the boundedness of the noise derivative since, in this paper, we primarily focus on addressing low-frequency noise. High-frequency noise components can*

be effectively attenuated through pre-filtering, and the residual noise is low-frequency noise that satisfies the boundedness condition of the noise derivative.

2.1. Global Reference System and Communication Topology

Suppose the states of the global reference system, which can be considered as a virtual leader, keep changing throughout the entire process, with dynamics described by

$$\begin{cases} \dot{\boldsymbol{z}}_r = \boldsymbol{A}_r \boldsymbol{z}_r, \\ \boldsymbol{x}_r = \boldsymbol{C}_r \boldsymbol{z}_r, \end{cases} \tag{4}$$

where $\boldsymbol{z}_r \in \mathbb{R}^2$ denote the leader's states, $\boldsymbol{x}_r \in \mathbb{R}$ is the leader's position, and $\boldsymbol{A}_r \in \mathbb{R}^{2\times 2}$ and $\boldsymbol{C}_r \in \mathbb{R}^{1\times 2}$ are the coefficient matrices.

The communication topology among the N UAVs is specified by a directed graph

$$\mathcal{G}(t) = \{\mathcal{V}(t), \mathcal{E}(t)\}, \tag{5}$$

where $\mathcal{V}(t) = \{v_0, v_1, \ldots, v_N\}$ denotes the vertex set of $\mathcal{G}$ and $\mathcal{E}(t) = \mathcal{V} \times \mathcal{V} = \{(i,j) : i,j \in \mathcal{V}\}$ is the time-varying edge set of $\mathcal{G}$. The vertex v_i represents the i-th follower and v_0 is the leader (i.e., global reference system). $\mathcal{A}(t) = [a_{ij}(t)] \in \mathbb{R}^{N\times N}$ is the adjacency matrix of the directed graph, and $a_{ij} \neq 0$ is equivalent to $(j,i) \in \mathcal{E}$, where $a_{ii} = 0$, and $a_{ij} = 1$ represents that the UAV v_i can obtain the information from its neighbor v_j at time t. The Laplacian matrix of the graph $\mathcal{G}(t)$ is defined as $\mathcal{L}(t) = [l_{ij}(t)] \in \mathbb{R}^{N\times N}$ with $l_{ii} = \sum_{j=1}^{N} a_{ij}$ and $l_{ij} = -a_{ij}$, $i \neq j$. Additionally, we introduce a matrix $\mathcal{B}(t) = \text{diag}\{b_{ii}(t)\} \in \mathbb{R}^{N\times N}$ to indicate the available communication between the leader and followers, where $b_{ii} = 1$ represents that the UAV v_i can obtain the leader's information at time t; otherwise, $b_{ii} = 0$.

Assumption 2 (see Assumption 5 in [25]). *There exists a subsequence $\{i_k\}$ of $\{i : i = 0, 1, \ldots\}$ with $t_{i_{k+1}} - t_{i_k} < \alpha$ for some positive α such that every node $i \in \mathcal{N} = \{1, \ldots, N\}$ is reachable from node 0 in the union graph $\bigcup_{j=i_k}^{i_{k+1}-1} \bar{\mathcal{G}}_{\sigma(t_j)}$.*

2.2. Control Objective

Define the state tracking error of each UAV as

$$\tilde{\boldsymbol{x}}_i = \boldsymbol{x}_r - \boldsymbol{x}_i. \tag{6}$$

The control objective of this paper is to design a controller u_i for each UAV such that the UAV can follow the leader whose dynamics are specified by (4) under the switching communication network $\mathcal{G}(t)$ in the presence of the measurement noise and input disturbance, and the tracking error of each UAV satisfies

$$\|\tilde{\boldsymbol{x}}_i(t)\| \leq \zeta(\varepsilon), \ \forall t > t_x, \tag{7}$$

where $\|\cdot\|$ denotes the Euclidean norm, ε is a tunable parameter, and $\zeta(\varepsilon)$ is the ultimate bound satisfying $\zeta(\varepsilon) \to 0$ as $\varepsilon \to 0$, t_x is the corresponding settling time.

3. Methodology

We now start addressing the issues of measurement noise and disturbance in multi-UAV-system consensus tracking control. To tackle these challenges, we propose a two-component control framework, whose construction is shown in Figure 1. We separate the consensus control for multi-UAV systems with measurement noise and disturbance into two procedures: (1) obtaining the reference from the communication network and

(2) designing the robust tracking controller to reject the measurement noise and disturbance. In the proposed control frame, we first introduce a distributed observer to generate the local reference, which is still effective under the switching communication network and is independent of each UAV's states. Having obtained the local reference, we design a local dual-estimator-based tracking controller by combining the UDE with MEE. This design enables the simultaneous rejection of measurement noise and disturbances, achieving high-precision tracking control.

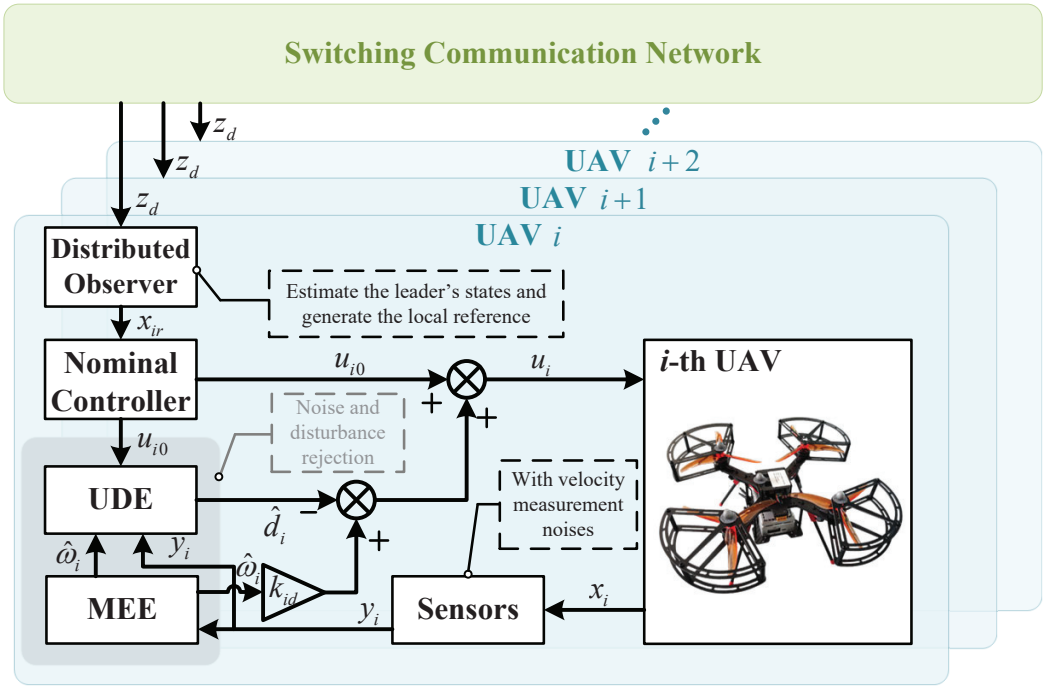


Figure 1. The proposed distributed control framework.

3.1. Distributed Observer Design

Since directly designing the consensus protocol for each UAV under the switching communication network and measurement noise is challenging, we first introduce the distributed observer [25] to estimate the leader's states and generate the local reference for followers. The distributed observer for each UAV is designed as

$$\begin{aligned} \dot{\hat{\boldsymbol{z}}}_i(t) &= \boldsymbol{A}_r \hat{\boldsymbol{z}}_i(t) + \mu_i \boldsymbol{e}_i(t), \\ \boldsymbol{e}_i(t) &= b_{ii}(t)\left[\boldsymbol{z}_r(t) - \hat{\boldsymbol{z}}_i(t)\right] + \sum_{j \in \mathcal{N}} a_{ij}(t)\left[\hat{\boldsymbol{z}}_j(t) - \hat{\boldsymbol{z}}_i(t)\right], \; i \in N, \end{aligned} \tag{8}$$

where $\boldsymbol{A}_r$ represents the coefficient matrix, $\hat{\boldsymbol{z}}_i \in \mathbb{R}^2$ denotes the estimation of the leader's states $\boldsymbol{z}_r$, $\boldsymbol{e}_i$ is the consensus estimation error, and μ_i is a tunable positive constant. Let $\boldsymbol{\xi}_i = \hat{\boldsymbol{z}}_i - \boldsymbol{z}_r \in \mathbb{R}^m$ represent the reference estimation error, and substituting (4) into (8), we have

$$\dot{\boldsymbol{\xi}}(t) = \left[\boldsymbol{I}_N \otimes \boldsymbol{A}_r - \mu\left(\mathcal{L}(t) \otimes \boldsymbol{I}_m + \mathcal{B}(t) \otimes \boldsymbol{I}_m\right)\right]\boldsymbol{\xi}(t), \tag{9}$$

where the notation $\otimes$ means the Kronecker product and $\boldsymbol{I}_N, \boldsymbol{I}_m$ are the identity matrices with corresponding dimensions. Then, the following lemma holds.

Lemma 1 (Lemma 2 in [25])**.** *Under the Assumption 2, for arbitrary $\mu > 0$, the estimation error $\boldsymbol{\xi}_i$ can converge to $\boldsymbol{0}_m$ exponentially, provided that $\boldsymbol{A}_r$ has no eigenvalues with positive real parts.*

The estimation provided by the distributed observer is independent of the UAVs' states, rendering a decoupling between the reference estimation and the controller design. This decoupling simplifies the subsequent controller design, allowing us to focus on the design of a single UAV controller that can effectively reject the measurement noise and input disturbance.

3.2. Classic UDE-Based Output Feedback Controller Design

To track the reference generated by the distributed observer, we subsequently design a controller that is capable of rejecting disturbance and measurement noise. Time-varying disturbances universally exist in industrial systems, including external disturbances and internal model uncertainties like unmodeled dynamics and parameter perturbations. Without loss of generality, we consider the lumped input disturbance in this paper, which lies in the same channel of the system input. The UDE is an effective tool for rejecting disturbances. It estimates the unknown disturbances based on measurable system states and inputs and then compensates for them. We will first design the classic UDE-based output feedback controller, which does not consider the measurement noise, and analyze its limitation in the presence of measurement noise. Subsequently, the MEE is designed to estimate the measurement noise and combined with UDE to simultaneously reject the noise and disturbance.

We add the superscript "′" to the variables to denote the corresponding states without considering the noise. Therefore, the classic UDE-based controller u_i' of each UAV is designed as

$$u_i' = \underbrace{u_{id} + k_{ip}\tilde{y}_{i1} + k_{id}\tilde{y}_{i2}'}_{u_{i0}} - \hat{d}_i', \tag{10}$$

where u_{id} is the feedforward term designed based on the model and reference, k_{ip} and k_{id} are the feedback gains, u_{i0} represents the nominal controller, $\tilde{y}_{i1} = x_{ir} - y_{i1}$ is the local position tracking error, $\tilde{y}_{i2}' = \dot{x}_{ir} - y_{i2}'$ is the local velocity tracking error without measurement noise (i.e., $y_{i2}' = x_{i2}$), and $\hat{d}'$ is the disturbance estimation term generated by UDE. Unlike other time-domain disturbance estimation algorithms presented in [26], the UDE is designed in the frequency domain and satisfies

$$\hat{D}_i'(s) = G_i^d(s) D_i(s). \tag{11}$$

In this paper, we use the uppercase letter to represent the frequency domain expression corresponding to the variable. Substituting (1) into (11) yields

$$\hat{D}_i'(s) = G_i^d(s)\Big[sY_{i2}'(s) - y_{i2}'(0) - \alpha_1 Y_{i1}(s) - \alpha_2 Y_{i2}'(s) - U_i'(s)\Big]. \tag{12}$$

The transfer function $G_i^d(s)$ is a designable low-pass filter and can be expressed as

$$G_i^d(s) = \frac{1}{T_{id}s + 1}, \tag{13}$$

where $T_{id} > 0$ is the UDE parameter. Plugging (10) into (12), one can obtain

$$\hat{D}_i'(s) = G_i^d(s)\Big[sY_{i2}'(s) - y_{i2}'(0) - \alpha_1 Y_{i1}(s) - \alpha_2 Y_{i2}'(s) - U_{id}(s) - k_{ip}\tilde{Y}_{i1}(s) - k_{id}\tilde{Y}_{i2}'(s) + \hat{D}_i'(s)\Big]. \tag{14}$$

Calculating $\hat{D}'_i(s)$ in (14) gives

$$\hat{D}'_i(s) = \frac{G^d_i(s)}{1 - G^d_i(s)} \left[sY'_{i2}(s) - y'_{i2}(0) - \alpha_1 Y_{i1}(s) - \alpha_2 Y'_{i2}(s) - U_{id}(s) - k_{ip}\tilde{Y}_{i1}(s) - k_{id}\tilde{Y}'_{i2}(s) \right]. \quad (15)$$

Finally, substituting (13) into (15), we have

$$\hat{D}'_i(s) = \frac{1}{T_{id}} Y'_{i2}(s) - \frac{1}{T_{id}s} \left[y'_{i2}(0) + \alpha_1 Y_{i1}(s) + \alpha_2 Y'_{i2}(s) + U_{id}(s) + k_{ip}\tilde{Y}_{i1}(s) + k_{id}\tilde{Y}'_{i2}(s) \right], \quad (16)$$

whose time-domain expression is

$$\hat{d}'_i(t) = \frac{1}{T_{id}} \left[y'_{i2} - t y'_{i2}(0) - \int_0^t \left(\alpha_1 y_{i1}(\tau) + \alpha_2 y'_{i2}(\tau) + u_{id}(\tau) + k_{ip}\tilde{y}_{i1}(\tau) + k_{id}\tilde{y}'_{i2}(\tau) \right) d\tau \right]. \quad (17)$$

However, when considering the measurement noise by replacing the term y'_{i2} with $y'_{i2} + \omega_i$ in both the controller (10) and UDE (17) and substituting (1) and (10) into (6), the system error dynamics can be derived as

$$\begin{aligned} \begin{bmatrix} \dot{\tilde{x}}_{i1} \\ \dot{\tilde{x}}_{i2} \end{bmatrix} &= \begin{bmatrix} 0 & 1 \\ \alpha_1 - k_{ip} & \alpha_2 - k_{id} \end{bmatrix} \begin{bmatrix} \tilde{x}_{i1} \\ \tilde{x}_{i2} \end{bmatrix} + \begin{bmatrix} 0 \\ -1 \end{bmatrix} \tilde{d}'_i + \begin{bmatrix} 0 \\ k_{id} + \frac{1}{T_{id}} \end{bmatrix} \omega_i \\ &+ \begin{bmatrix} 0 \\ -\frac{1}{T_{id}} \end{bmatrix} t\omega_i(0) + \begin{bmatrix} 0 \\ \frac{k_{id} - \alpha_2}{T_{id}} \end{bmatrix} \int_0^t \omega_i(\tau) d\tau, \end{aligned} \quad (18)$$

where $\tilde{d}'_i = d_i - \hat{d}'_i$ is the estimation error of the UDE without measurement noise and satisfies

$$\dot{\tilde{d}}'_i = -\frac{1}{T_{id}} \tilde{d}'_i + \dot{d}_i, \quad (19)$$

by noting the UDE design process (11).

From the dynamics in (18) and (19), we observe a trade-off between disturbance rejection and control performance in the presence of the measurement noise. Specifically, while decreasing the UDE parameter T_d extends the bandwidth of disturbance estimation, it can also magnify the measurement noise, thereby degrading the system control performance. To address this limitation, we have designed a MEE inspired by the UDE design process. By combining MEE with UDE, the controller can simultaneously reject both noise and disturbance.

3.3. MEE Design

To address the measurement noise issue, we introduce the MEE [27] to the controller to actively estimate and compensate for the measurement noise. The noise estimation signal is formulated as

$$\hat{\Omega}_i(s) = G^\omega_i(s)\Omega_i(s), \quad (20)$$

where $\hat{\omega}_i$ is the estimation of the measurement noise ω_i,and $G^\omega_i(s)$ is a strictly proper filter to ensure the estimation is physically realizable. Accordingly, we design $G^\omega_i(s)$ as

$$G^\omega_i(s) = \frac{1}{T_{i\omega}s + 1}, \quad (21)$$

where $T_{i\omega} > 0$ is a tunable MEE parameter determining the filter bandwidth. Substituting (2) into (20) yields

$$\hat{\Omega}_i(s) = G^\omega_i(s)\left[Y_2(s) - sY_1(s) + y_1(0) \right]. \quad (22)$$

Furthermore, Substituting (21) into (22) produces

$$\hat{\Omega}_i(s) = \frac{1}{T_{i\omega}s+1}\left[Y_{i2}(s) + y_{i1}(0)\right] - \frac{s}{T_{i\omega}s+1}Y_{i1}(s). \tag{23}$$

It can be observed that, in (23), after adding the filter $G_i^{\omega}(s)$, the original unrealizable differential term $sY_{i1}(s)$ is replaced with the realizable numerical differential $\frac{s}{T_{i\omega}s+1}Y_{i1}(s)$.

3.4. UDE+MEE-Based Output Feedback Controller Design

Having completed the MEE design, we combined it with a nominal controller and UDE to simultaneously reject the measurement noise and input disturbance. The control input u_i of the UDE+MEE-based output feedback controller is designed as

$$\begin{aligned} u_i &= u_{id} + k_{ip}\tilde{y}_{i1} + k_{id}\left[x_{i2d} - (y_{i2} - \hat{\omega}_i)\right] - \hat{d}_i, \\ &= u_{id} + k_{ip}\tilde{y}_{i1} + k_{id}(\tilde{y}_{i2} + \hat{\omega}_i) - \hat{d}_i, \end{aligned} \tag{24}$$

wherein we use noise estimation $\hat{\omega}_i$ to reject the noise in velocity feedback. Similar to the classic UDE design process (12), the modified UDE is given by

$$\hat{D}_i(s) = G_i^d(s)\left[s\left(Y_{i2}(s) - \hat{\Omega}_i(s)\right) - y_{i2}(0) - \alpha_1 Y_{i1}(s) - \alpha_2\left(sY_{i1}(s) - y_{i1}(0)\right) - U_i(s)\right], \tag{25}$$

where we replace the term $sY_{i2}(s)$ with $s\left(Y_{i2}(s) - \hat{\Omega}(s)\right)$ and replace $\alpha_2 Y_{i2}(s)$ with $\alpha_2\left(sY_{i1}(s) - y_{i1}(0)\right)$ to mitigate the impact of noise on the UDE. The replacement of $\alpha_2 Y_{i2}(s)$ is equivalent and can be realized by UDE, while the replacement of $sY_{i2}(s)$ uses the noise estimation $\hat{\omega}_i$ to compensate for the velocity measurement. Substituting (13) and (24) into (25) yields

$$\begin{aligned} \hat{D}_i(s) = \frac{1}{T_{id}}\left[-\alpha_2 Y_{i1}(s) + Y_{i2}(s) - \hat{\Omega}_i(s)\right] + \frac{1}{T_{id}s}\left[-\alpha_1 Y_{i1}(s) + \alpha_2 y_{i1}(0) - y_{i2}(0) - U_{id}(s)\right. \\ \left. -k_{ip}\tilde{Y}_{i1}(s) - k_{id}\tilde{Y}_{i2}(s) - k_{id}\hat{\Omega}_i(s)\right]. \end{aligned} \tag{26}$$

Plugging $\hat{\Omega}(s)$ (23) into (26), we have

$$\begin{aligned} \hat{D}(s) = \frac{1}{T_{id}}\left[\left(1 - \frac{s+k_{id}}{T_{i\omega}s^2+s}\right)Y_{i2}(s) + \left(\frac{s+k_{id}}{T_{i\omega}s+1} - \alpha_2 - \frac{\alpha_1}{s}\right)Y_{i1}(s)\right] + \frac{1}{T_{id}s}\left[\left(\alpha_2 - \frac{s+k_{id}}{T_{i\omega}s+1}\right)y_{i1}(0)\right. \\ \left. -y_{i2}(0) - U_{id}(s) - k_{ip}\tilde{Y}_{i1}(s) - k_{id}\tilde{Y}_{i2}(s)\right]. \end{aligned} \tag{27}$$

4. Stability and Performance Analysis

In this section, the stability of the proposed controller is proved and the relationship between the controller parameter and system control performance is revealed by the singular perturbation theorem.

4.1. Stability Proof

Suppose the UAV has obtained the leader's states by the distributed observer, substituting (1) and (24) into (6); the error system is derived as

$$\begin{bmatrix} \dot{\tilde{x}}_{i1} \\ \dot{\tilde{x}}_{i2} \end{bmatrix} = \begin{bmatrix} 0 & 1 \\ \alpha_1 - k_{ip} & \alpha_2 - k_{id} \end{bmatrix}\begin{bmatrix} \tilde{x}_{i1} \\ \tilde{x}_{i2} \end{bmatrix} + \begin{bmatrix} 0 \\ -1 \end{bmatrix}\tilde{d}_i + \begin{bmatrix} 0 \\ k_{id} \end{bmatrix}\tilde{\omega}_i, \tag{28}$$

where $\tilde{\omega}_i = \omega_i - \hat{\omega}_i$ is the noise estimation error.

Theorem 1. *Under the stability condition $k_{ip} > \alpha_1$ and $k_{id} > \alpha_2$, the closed-loop system (28) is input-to-state-stable (ISS).*

Proof of Theorem 1. By noting the error dynamics (28), the estimation error term $\tilde{d}_i$ and $\tilde{\omega}_i$ can be regarded as the input of the unforced subsystem

$$\begin{bmatrix} \dot{\tilde{x}}_{i1} \\ \dot{\tilde{x}}_{i2} \end{bmatrix} = \underbrace{\begin{bmatrix} 0 & 1 \\ \alpha_1 - k_{ip} & \alpha_2 - k_{id} \end{bmatrix}}_{A_i^*} \begin{bmatrix} \tilde{x}_{i1} \\ \tilde{x}_{i2} \end{bmatrix}. \tag{29}$$

According to the Lemma 4.6 in [28], the system (28) is ISS if the unforced subsystem (29) has a globally exponentially stable equilibrium point at the origin $\tilde{\boldsymbol{x}}_i = \mathbf{0}$. Under the stability condition $k_{ip} > \alpha_1$ and $k_{id} > \alpha_2$, the matrix A_i^* is Hurwitz, which indicates the unforced system has a globally exponentially stable equilibrium point at the origin. Therefore, the error system (28) is ISS. The proof is complete. □

4.2. Performance Analysis

Theorem 2. *The measurement noise and external disturbance rejection performance can be simultaneously improved by tuning a single parameter ε. The control objective (7) can be achieved under Assumption 1.*

Proof of Theorem 2. For simplicity, we omit the subscript for each variable in performance analysis, and the results are appropriate to all UAVs. Considering the following parameter mapping $T_\omega = \varepsilon T_\omega^*$, $T_d = \varepsilon T_d^*$, where $\varepsilon > 0$ is the singular perturbation parameter and T_ω^*, T_d^* are the tunable parameters.

Remark 2. *This parameter mapping can unify tuning the MEE and UDE parameters into tuning a single parameter ε, which simplifies the multi-parameter optimization problem when using the proposed methodology in practice.*

According to the MEE design process (20) and (21), the noise estimation error is

$$\dot{\tilde{\omega}} = -\frac{1}{T_\omega}\tilde{\omega} + \dot{\omega}. \tag{30}$$

Moreover, combining (12), (19) and (25) gives the disturbance estimation error as

$$\tilde{D}(s) = \frac{T_d s}{T_d s + 1} D(s) - \frac{s}{T_d s + 1}\tilde{\Omega}(s) + \frac{1}{T_d s + 1}\omega(0), \tag{31}$$

where $\tilde{D}(s) = D(s) - \hat{D}(s)$ is the UDE estimation error. Plugging (30) into (31) and transferring the result into the time-domain yields

$$\dot{\tilde{d}} = -\frac{1}{T_d}\tilde{d} + \frac{1}{T_d T_\omega}\tilde{\omega} - \frac{1}{T_d}\dot{\omega} + \dot{d} + \frac{1}{T_d}\omega(0). \tag{32}$$

Then, conducting the parameter mapping given by (33), the estimation error (30) and (32) can be rewritten as

$$\begin{aligned} \varepsilon\dot{\tilde{\omega}} &= -\frac{1}{T_\omega^*}\tilde{\omega} + \varepsilon\dot{\omega} \\ \varepsilon^2\dot{\tilde{d}} &= -\frac{\varepsilon}{T_d^*}\tilde{d} + \frac{1}{T_d^* T_\omega^*}\tilde{\omega} - \frac{\varepsilon}{T_d^*}\dot{\omega} + \varepsilon^2\dot{d} + \frac{\varepsilon}{T_d^*}\omega(0). \end{aligned} \tag{33}$$

Considering the following auxiliary parameter

$$\lambda_1 = \tilde{\omega}, \quad \lambda_2 = \varepsilon \tilde{d}, \tag{34}$$

estimation dynamics (33) is further expressed as

$$\varepsilon \begin{bmatrix} \dot{\lambda}_1 \\ \dot{\lambda}_2 \end{bmatrix} = \begin{bmatrix} -\frac{1}{T_\omega^*} & 0 \\ \frac{1}{T_d^* T_\omega^*} & -\frac{1}{T_d^*} \end{bmatrix} \begin{bmatrix} \lambda_1 \\ \lambda_2 \end{bmatrix} + \begin{bmatrix} \varepsilon \dot{\omega} \\ -\frac{\varepsilon}{T_d^*} \dot{\omega} + \varepsilon^2 \dot{d} + \frac{\varepsilon}{T_d^*} \omega(0) \end{bmatrix}. \tag{35}$$

Then, the tracking error dynamics (28) and estimation error dynamics (35) can be rewritten into the standard singular perturbation form, where the tracking error is regarded as the slow dynamics, while noise and disturbances estimation error represent the fast dynamics.

We can readily verify that the demands of Theorem 11.2 in [28] are all satisfied provided Assumption 1. Hence, there exists $\varepsilon^*, k_1, k_2 > 0$ such that $\forall\ 0 < \varepsilon < \varepsilon^*$ and any $t_b > 0$; we have

$$\|\tilde{\boldsymbol{x}}(t) - \tilde{\boldsymbol{x}}_r(t)\| \leq k_1 \varepsilon, \quad \forall\ t > 0, \tag{36}$$

$$\|\boldsymbol{\lambda}(t) - \boldsymbol{h}[t, \boldsymbol{x}_r(t)]\| \leq k_2 \varepsilon, \quad \forall\ t > t_b, \tag{37}$$

where $\tilde{\boldsymbol{x}}_r(t) = e^{\boldsymbol{A}^*} \tilde{\boldsymbol{x}}(0)$ denotes the reduced model's solution, whose expression is consistent with the unforced subsystem (29) and $\boldsymbol{h}[t, \boldsymbol{x}_r(t)] = \boldsymbol{0}$ is the quasi-steady state of (35) under the condition $\varepsilon = 0$.

Since the matrix $\boldsymbol{A}^*$ is Hurwitz, there exists a specific bound $\bar{\tilde{x}}$ and a settling time t_x satisfying

$$\|\tilde{\boldsymbol{x}}_r(t)\| \leq \bar{\tilde{x}}, \quad \forall\ t > t_x. \tag{38}$$

Therefore, the following inequality holds

$$\|\tilde{\boldsymbol{x}}(t)\| \leq \|\tilde{\boldsymbol{x}}(t) - \tilde{\boldsymbol{x}}_r(t)\| + \|\tilde{\boldsymbol{x}}_r(t)\| \leq k_1 \varepsilon + \bar{\tilde{x}}, \quad \forall\ t > t_x.$$

Thus, the control objective can be achieved under

$$0 < \varepsilon < \min\{\varepsilon^*, \frac{\zeta(\varepsilon) - \bar{\tilde{x}}}{k_1}\}. \tag{39}$$

For fast dynamics (37), we have

$$\|\boldsymbol{\lambda}(t) - \boldsymbol{0}\| \leq k_2 \varepsilon, \quad \forall\ t > t_b. \tag{40}$$

From the above inequality, we conclude that with the reduction of parameter ε, the noise and disturbance estimation errors can be reduced simultaneously. The proof is complete. □

Remark 3. *The parameter tuning guidelines for the proposed framework are summarized as follows. Specifically, thanks to the distributed structure of the controller, parameter tuning in practical applications can be divided into three simple procedures: firstly, tuning the parameter μ_i to ensure the rapid convergence of the leader's state estimation; secondly, tuning the feedback gain k_{ip} and k_{id} to ensure the stability of the tracking controller; finally, in accordance with Theorem 2, monotonically reducing the parameter ε to improve the noise and disturbance rejection ability. However, the value of ε may have a lower bound in practice due to the actuator bandwidth limitation and the need to prevent large overshoot during the initial control phase.*

5. Simulation Study on a Quadrotor Model

In this section, the consensus tracking control of quadrotors is carried out using Matlab/Simulink to verify the feasibility of the proposed control framework. To this end, we begin by modeling the dynamics of the quadrotor.

As shown in Figure 2, two frames are introduced to describe the translation and rotation of the quadrotor: the body frame $B = \{x_B, y_B, z_B\}$ and the inertial frame $I = \{x_I, y_I, z_I\}$. The body frame is fixed to the quadrotor, with the x_B-axis pointing forward, the y_B-axis to the right, and the z_B-axis pointing downward. The attitude of the quadrotor is specified by the Euler angles $\boldsymbol{\Theta} = [\phi, \theta, \psi] \in \mathbb{R}^3$, which represent the roll angle, pitch angle, and yaw angle, respectively. The transformation from the body frame to the inertial frame is facilitated by the rotation matrix

$$\boldsymbol{R}_B^I = \begin{bmatrix} \cos\theta\cos\psi & \sin\phi\cos\theta\cos\psi - \cos\phi\sin\psi & \sin\phi\sin\psi + \cos\phi\sin\theta\cos\psi \\ \cos\theta\sin\psi & \cos\phi\cos\psi + \sin\phi\sin\theta\sin\psi & \cos\phi\sin\theta\sin\psi - \sin\phi\cos\psi \\ -\sin\theta & \sin\phi\cos\theta & \cos\phi\cos\theta \end{bmatrix}. \quad (41)$$

We add the superscript to variables to denote its corresponding frame; e.g., $\boldsymbol{p}^I$ represents the quadrotor position in the inertial frame. Since the thrust of the quadrotor is perpendicular to the quadrotor body, by Newton's Second Law, the translational motion of the quadrotor can be modeled as

$$\ddot{\boldsymbol{p}}^B = \boldsymbol{R}_I^B \boldsymbol{\eta} g - \frac{1}{m_q} \boldsymbol{\eta} T - \mathscr{W}^B \times \dot{\boldsymbol{p}}^B + \boldsymbol{F}_d^B \quad (42)$$

where $\ddot{\boldsymbol{p}}^B \in \mathbb{R}^3$ is the quadrotor acceleration, $\boldsymbol{R}_I^B = (\boldsymbol{R}_B^I)^{-1}$ denotes the rotation matrix from the inertial frame to the body frame, $\boldsymbol{\eta} = [0, 0, 1]^T \in \mathbb{R}^3$ is the direction vector, $g \in \mathbb{R}$ is the gravitational acceleration, $m_q \in \mathbb{R}$ is the quadrotor mass, $T \in \mathbb{R}$ is the thrust generated by the motors, $\mathscr{W}^B = [p, q, r]^T \in \mathbb{R}^3$ is the angular velocity, and $\boldsymbol{F}_d^B \in \mathbb{R}^3$ represents air drag.

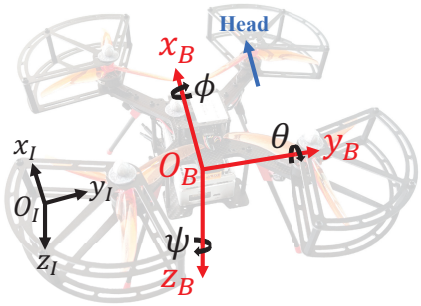


Figure 2. The quadrotor structure and frame setup.

According to Euler's rotation equations [29–31], the angular motion of the quadrotor is given by

$$\boldsymbol{J}^B \dot{\mathscr{W}}^B = \boldsymbol{\tau}^B - \mathscr{W}^B \times \left(\boldsymbol{J}^B \mathscr{W}^B\right), \quad (43)$$

where $\boldsymbol{J}^B = \mathrm{diag}(J_{xx}^B, J_{yy}^B, J_{zz}^B) \in \mathbb{R}^{3\times 3}$ is the quadrotor inertial tensor matrix and $\boldsymbol{\tau} \in \mathbb{R}^3$ is the torque generated by motors. The relationship between the angular velocity $\mathscr{W}^B$ and Euler angles $\boldsymbol{\Theta}$ is described by

$$\begin{bmatrix} \dot{\phi} \\ \dot{\theta} \\ \dot{\psi} \end{bmatrix} = \begin{bmatrix} 1 & \sin\phi\tan\theta & \cos\phi\tan\theta \\ 0 & \cos\phi & -\sin\phi \\ 0 & \sin\phi\sec\theta & \cos\phi\sec\theta \end{bmatrix} \begin{bmatrix} p \\ q \\ r \end{bmatrix}. \quad (44)$$

Under the small angle assumption

$$\sin\theta = \sin\phi = 0, \quad \cos\theta = \cos\phi = 1 \tag{45}$$

applied to the angular motion (43) and (44), and using the point-mass assumption on the translational motion (42), the dynamics of the quadrotor can be approximated as

$$\begin{aligned} \ddot{\boldsymbol{\Theta}} &= \left(\boldsymbol{J}^B\right)^{-1}\left(\boldsymbol{\tau}^B - \dot{\boldsymbol{\Theta}} \times (\boldsymbol{J}^B\dot{\boldsymbol{\Theta}})\right), \\ \ddot{\boldsymbol{p}}^I &= \boldsymbol{R}_B^I\ddot{\boldsymbol{p}}^B = \boldsymbol{\eta g} - \boldsymbol{R}_B^I\left(\frac{1}{m_q}\boldsymbol{\eta} T - \boldsymbol{F}_d^B\right). \end{aligned} \tag{46}$$

By utilizing the feedback linearization technique on (46) and considering velocity measurement noise, we obtain the simplified quadrotor model with measurement noise:

$$\ddot{\boldsymbol{\Xi}} = \boldsymbol{u} + \boldsymbol{d}, \tag{47}$$

$$\boldsymbol{v}^I = \dot{\boldsymbol{p}}^I + \boldsymbol{\omega}^I, \tag{48}$$

where $\boldsymbol{\Xi}^T = [\boldsymbol{\Theta}^T, (\boldsymbol{p}^I)^T]$, $\boldsymbol{v}^I$ denotes the measured quadrotor velocity, $\dot{\boldsymbol{p}}^I$ is the true quadrotor velocity, $\boldsymbol{\omega}^I \in \mathbb{R}^3$ is the velocity measurement noise, $\boldsymbol{u}^T = \left[\left(\boldsymbol{J}^{-B}\boldsymbol{\tau}^B\right)^T, \left(-\frac{1}{m_q}\boldsymbol{R}_B^I\boldsymbol{\eta}T + \boldsymbol{\eta g}\right)^T\right] = [u_x, u_y, u_z, u_\phi, u_\theta, u_\psi]$ is the control input, and $\boldsymbol{d}^T = \left[\left(\boldsymbol{R}_B^I\boldsymbol{F}_d^B\right)^T, \left(-\boldsymbol{J}^{-B}\cdot(\dot{\boldsymbol{\Theta}} \times (\boldsymbol{J}^B\dot{\boldsymbol{\Theta}}))\right)^T\right]$ denotes the external disturbance.

In the simulation, we employ the classic dual-loop control scheme for the quadrotor as shown in Figure 3. Here, $\phi_d, \theta_d, \psi_d \in \mathbb{R}$ represent the desired attitude angles, and $\varpi \in \mathbb{R}^4$ denotes the rotor speeds. To avoid collisions, the height reference for each quadrotor is set at different constant values. The quadrotors are required to achieve consensus in both the X- and Y-axes while maintaining their respective height references. Specifically, the outer-loop horizontal position controller is designed using the proposed control framework, while the altitude controller and inner-loop attitude controller are designed using conventional methods.

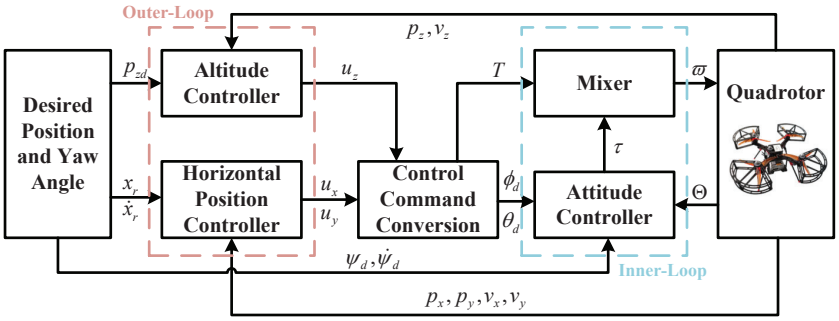


Figure 3. The quadrotor inner–outer-loop control scheme.

Rewriting the quadrotor translational motion in (47), and velocity measurement (48) into the standard state-space form, we have

$$\dot{\boldsymbol{x}}_k = \boldsymbol{A}\boldsymbol{x}_k + \boldsymbol{B}(u_k + d_k), \tag{49}$$

$$\boldsymbol{y}_k = \boldsymbol{C}\boldsymbol{x}_k + \boldsymbol{D}\omega_k, \quad k = x,\ y,\ z, \tag{50}$$

where $\boldsymbol{x}_k = [p_k^I, \dot{p}_k^I]^T \in \mathbb{R}^2$ is the quadrotor states along the k-axis, and $\boldsymbol{y}_k = [p_k, v_k]^T \in \mathbb{R}^2$ represents the measured quadrotor states. The quadrotor translational model (49) and (50) are consistent with the considered multi-UAV systems (1) and (2) by letting $\alpha_1 = 0,\ \alpha_2 = 0$.

Take the X-axis for example; the reference (4) is $\boldsymbol{x}_r = [p_{xd}, \dot{p}_{xd}]^T$, representing the desired position and velocity. The matrix $\boldsymbol{A}_r$ and $\boldsymbol{C}_r$ is

$$\boldsymbol{A}_r = \begin{bmatrix} 0 & 1 \\ -0.16 & 0 \end{bmatrix},\ \boldsymbol{C}_r = \begin{bmatrix} 1 & 0 \end{bmatrix}, \tag{51}$$

and $\boldsymbol{z}_r(0) = [0,\ 0.4]^T$. The reference design process of the Y-axis is similar to that of the X-axis. The initial states of the four quadrotors are $\boldsymbol{p}_1 = [0,\ 0,\ 1]^T$, $\boldsymbol{p}_2 = [0,\ 0,\ 2]^T$, $\boldsymbol{p}_3 = [0,\ 0,\ 3]^T$, $\boldsymbol{p}_4 = [0,\ 0,\ 4]^T$, and $\hat{\boldsymbol{z}}_i(0) = [0, 0]^T$. All the quadrotors have no velocity at the initial time. The model parameters and control gains are listed in Table 1.

Table 1. Model parameter and control gains in the simulation.

Symbol	Parameter Description	Value
m_q	Quadrotor mass	1 kg
g	Gravitational acceleration	9.8 m/s^2
J_{xx}, J_{yy}, J_{zz}	Quadrotor moment of inertia	0.01 kg· m^2
μ_i	Gain of Distributed Observer	20
k_{ip}	Position feedback gain of local controller in X- and Y-axes	1.3
k_{id}	Velocity feedback gain of local controller in X- and Y-axes	1.8
T_{id}	UDE parameter in X- and Y-axes	0.2
$T_{i\omega}$	MEE parameter in X- and Y-axes	0.02

Figure 4 depicts the topology considered in the simulation, where nodes $1, 2, 3, 4$ represent the four quadrotors; the green node 0 is the leader; and the arrows indicate the communication links between the quadrotors. The dwell time of each stage is 2.5 s.

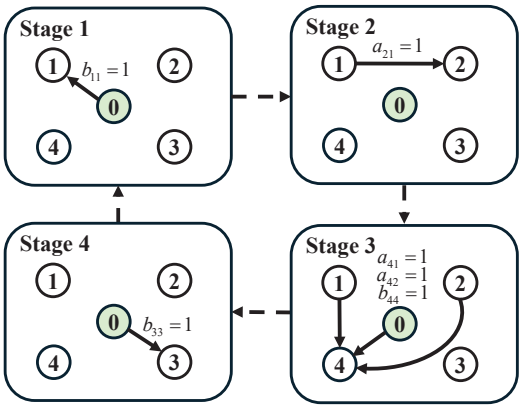
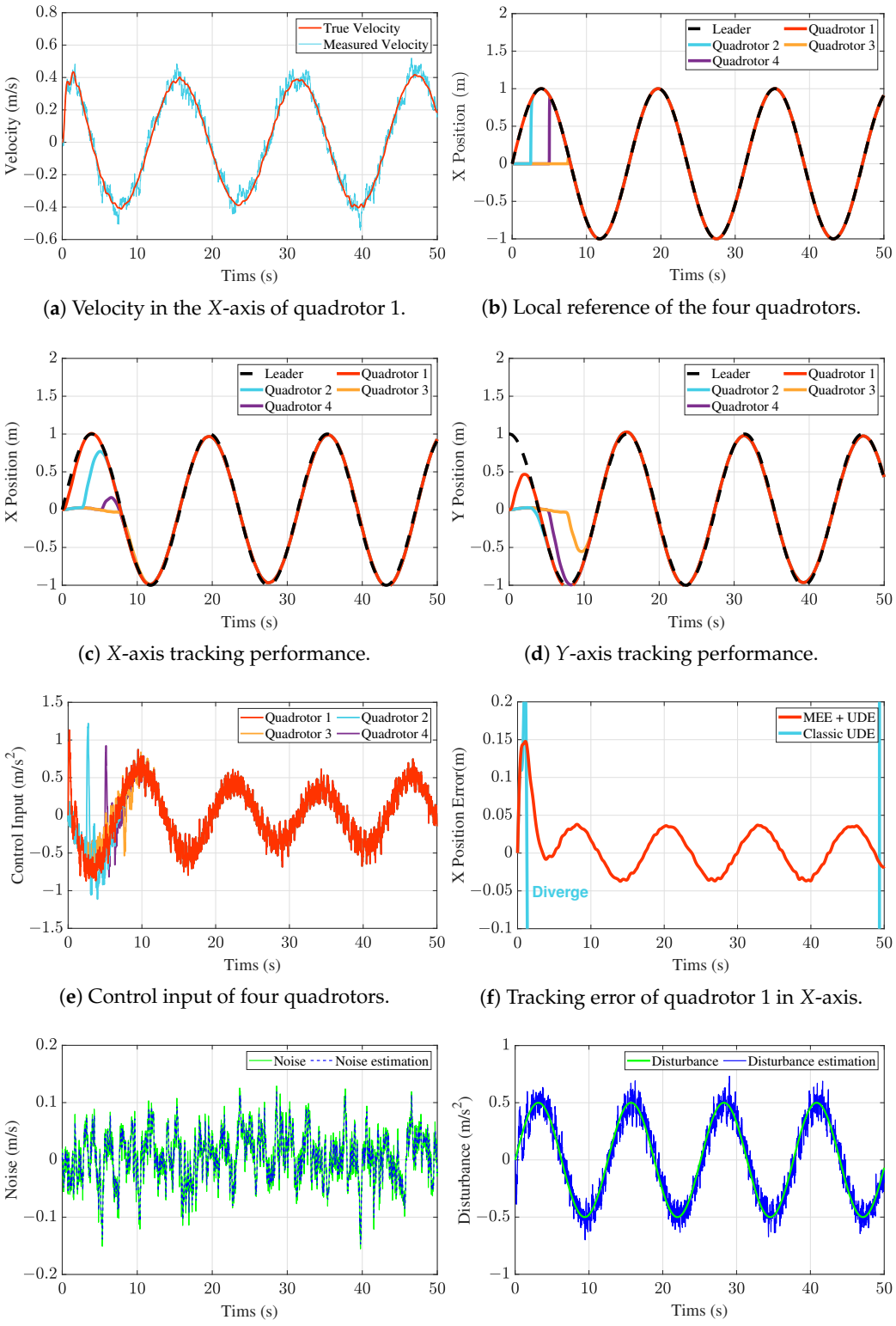


Figure 4. The considered communication topology in simulation.

Figure 5 shows the simulation results of the proposed control framework. The time-varying external disturbances of four quadrotors are set as $d_i(t) = 0.5sin(0.5t)$. To simulate the sensor measurement noise, Gaussian-distributed noise with a mean of 0 and variance of 1 is passed through a low-pass filter and subsequently added to quadrotor velocity feedback, as illustrated in Figure 5a. Figure 5b is the local reference generated from the distributed observer, indicating that quadrotor 2 obtains the leader's states at 2.5 s, while quadrotors 3 and 4 can access the leader at 5 s and 7.5 s, respectively. Figure 5c,d demonstrate the tracking performance of the four quadrotors along the X- and Y-axes. Despite the presence of measurement noise and disturbance, the proposed control framework effectively rejects

them; therefore, the quadrotor can achieve high-precision consensus tracking. Figure 5f compares the proposed dual-estimators-based robust controller with the classic UDE-based controller under the same controller parameters, for which we can observe that the classic UDE diverges. Figure 5g,h show the noise and disturbance estimations, respectively.



(**a**) Velocity in the *X*-axis of quadrotor 1.

(**b**) Local reference of the four quadrotors.

(**c**) *X*-axis tracking performance.

(**d**) *Y*-axis tracking performance.

(**e**) Control input of four quadrotors.

(**f**) Tracking error of quadrotor 1 in *X*-axis.

(**g**) Noise estimation of quadrotor 1.

(**h**) Disturbance estimation of quadrotor 1.

Figure 5. Results of simulation on the quadrotor model.

6. Experimental Verification on the Reduced Quadrotor Platform

Since the numerical simulation cannot reflect the key properties of a quadrotor (particularly the sensor measurement errors addressed in this paper), we implement the experiments on a reduced quadrotor platform (half-quadrotor model) equipped with the same types of onboard sensors as a real quadrotor, such as accelerators and gyroscopes. Figure 6 depicts the coordinate definition and components of the platform [32]. This device has two degrees of freedom: pitch angle θ and yaw angle ψ. In the experiments, we fix the yaw angle and only control the pitch angle to validate the proposed control framework in the quadrotor attitude control.



Figure 6. The reduced quadrotor experimental platform (Quanser Aero 2).

6.1. Reduced Quadrotor Model

In the experiments, we assume that all devices have identical model parameters. The model of the reduced quadrotor model pitch channel angle is given by

$$J_p\ddot{\theta}_i + D_p\dot{\theta}_i + K_{sp}\theta_i = \tau_{ip}, \tag{52}$$

where $J_p \in \mathbb{R}^+$ is the total moment of inertia, $D_p \in \mathbb{R}^+$ is the damping coefficient, $K_{sp} \in \mathbb{R}^+$ is the stiffness coefficient, and $\tau_{ip} \in \mathbb{R}$ is the torque generated by motors. We can readily transform the model (52) into the standard form (1) and (2) by letting $\alpha_1 = -K_{sp}/J_p$, $\alpha_2 = -D_p/J_p$, $u = \tau_{ip}/J_p$, $x_{i1} = y_{i1} = \theta_i$, $x_{i2} = \dot{\theta}_i$, $y_{i2} = \dot{\theta}_i + \omega_i$. The external disturbance and model uncertainty are treated as lumped input disturbance d_i.

The model (52) parameters are identified as $J_p = 0.0232$, $D_p = 0.0020$, $K_{sp} = 0.0200$. Additionally, we find through experiments that the classic linear actuator model $\tau_p = K_{pp}V_{ip}$, where V_{ip} is the voltage and K_{pp} denotes the torque thrust gain, cannot precisely describe the actuator model due to the nonlinearity in the thrust and motor rotation speed relationship. To construct a better model for the actuator, we collect the τ_{ip} and V_{ip} around the different equilibria and use the following nonlinear function to fit the collected data.

$$V_{ip} = \left(p_1\tau_p^3 + p_2\tau_p^2 + p_3\tau_p + p_4\right)\sqrt{\tau}_{ip}. \tag{53}$$

Matlab Curve Fitting Toolbox is utilized to fit the curve, and the parameters in (53) are identified as $p_1 = -141300$, $p_2 = 24150$, $p_3 = -1249$, $p_4 = 114.2$. Figure 7 shows the fitting results, from which we can observe that the relationship between the τ_p and V_p is strongly nonlinear, and the fitted result can effectively describe this relationship.

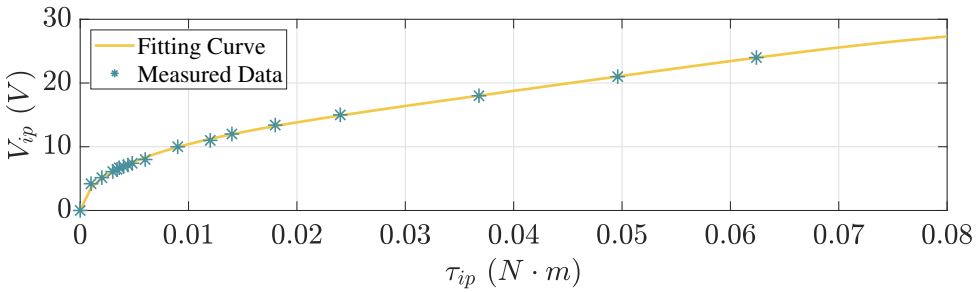


Figure 7. Actuator fitting result.

6.2. Experimental Setup

The reference system (4) is $\boldsymbol{x}_r = [\theta_r, \dot{\theta}_r]^T$ in the experiments, and the dynamics of this virtual leader are specified by

$$\boldsymbol{A}_r = \begin{bmatrix} 0 & 1 \\ -1 & 0 \end{bmatrix}, \quad \boldsymbol{C}_r = \begin{bmatrix} 0.2 & 0 \end{bmatrix}. \tag{54}$$

Therefore, the feedforward term in the controller (24) can be calculated as

$$u_{id} = \boldsymbol{C}_r \boldsymbol{A}_r \boldsymbol{A}_r \hat{\boldsymbol{z}}_i - \alpha_1 \boldsymbol{C}_r \hat{\boldsymbol{z}}_i - \alpha_2 \boldsymbol{C}_r \boldsymbol{A}_r \hat{\boldsymbol{z}}_i. \tag{55}$$

We add a $0.2rad$ offset to the system, and the initial states of the system are given by $\theta_i(0) = 0$ rad, $\dot{\theta}_i(0) = 0$ rad/s, $\hat{\boldsymbol{z}}_i(0) = [0,0]^T$, $\boldsymbol{z}_r(0) = [-1,0]^T$. Under this initial condition, the trajectory of the leader is $\theta_r(t) = 0.2 + 0.2sin(t - \frac{\pi}{2})$ rad. The parameters of the proposed control framework are selected as $\mu_i = 20$, $k_{ip} = 5$, $k_{id} = 3$, $T_{i\omega} = 0.1$, $T_{id} = 0.1$.

Figure 8 shows the communication topology considered in the experiments where the dwell time of each stage is 5 s, with a communication interruption occurring in Stage 4. Moreover, to validate the effectiveness of the proposed control framework, two robust output controllers, ESO-based and RISE-based, are implemented in the experiments. These two controllers address noise measurement from different perspectives. The ESO-based controller estimates the angle velocity and does not use the measured angular velocity in the feedback loop, while the RISE-based controller only relies on the angle feedback to stabilize the system. Three cases are designed in the experiments. In Case 1, we assume that all the quadrotors can obtain the information directly from the leader, while in Cases 2 and 3, the communication topology of the quadrotors is specified in Figure 8. In Case 2, an external disturbance is introduced to one quadrotor after all the quadrotors are synchronized to verify the robustness of the proposed control framework. To verify Theorem 2, in Case 3, we select the different values of ε in the experiments to compare their control performance.

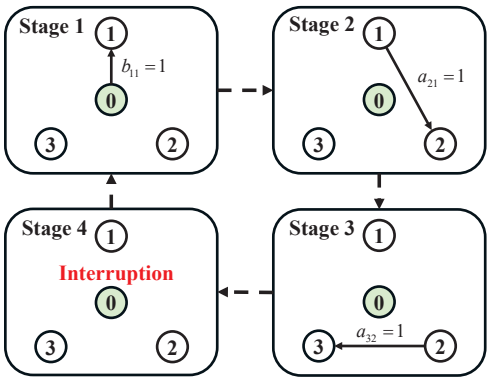
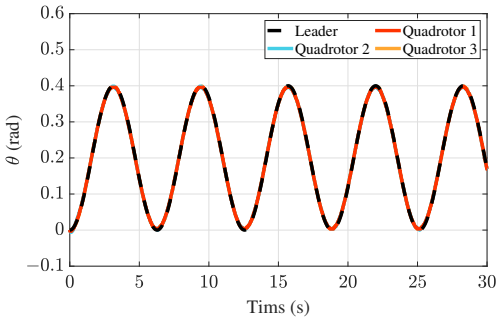


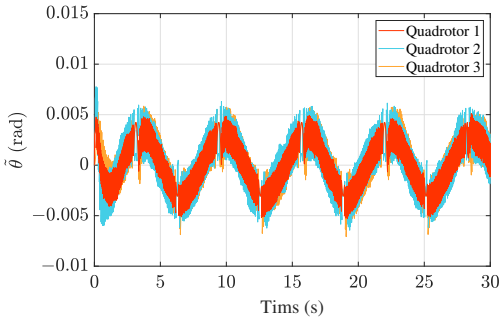
Figure 8. The considered communication topology in experiment.

6.3. Case 1: Consensus Tracking Under a Known Leader's States

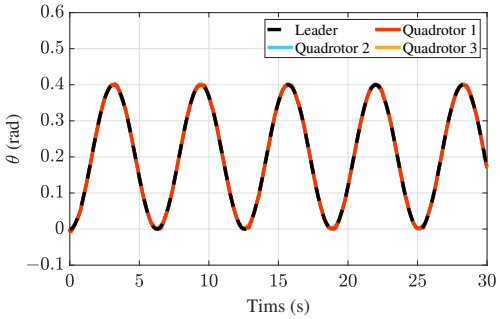
In this case, to verify the feasibility of the proposed local MEE+UDE-based tracking controller, all quadrotors can obtain the leader's states at the initial time. Figure 9 depicts the experimental results of Case 1. It can be observed that all three methods achieve consensus tracking. The performance of the RISE-based controller differs little from the MEE+UDE-based controller, while the ESO-based controller performs large torque commands.



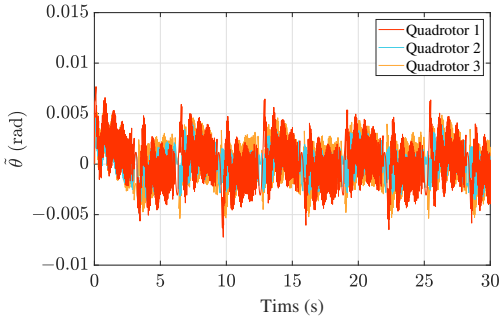
(**a**) Trajectory of MEE+UDE.



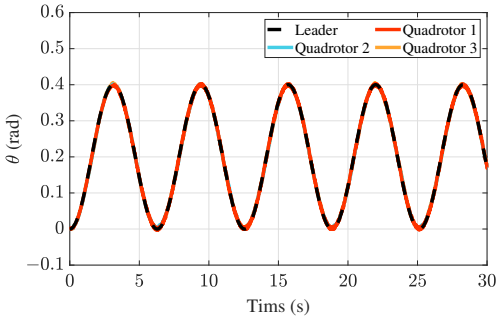
(**b**) Tracking error of MEE+UDE.



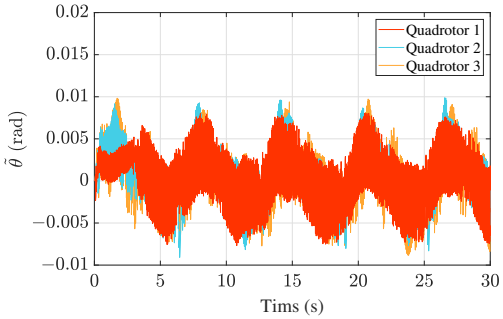
(**c**) Trajectory of RISE.



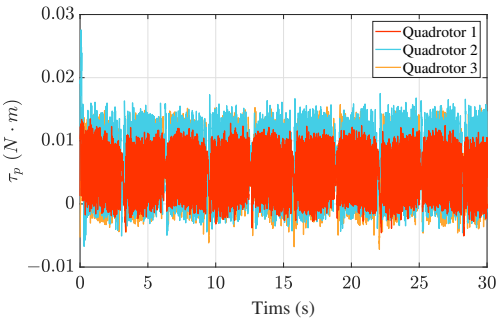
(**d**) Tracking error of RISE.



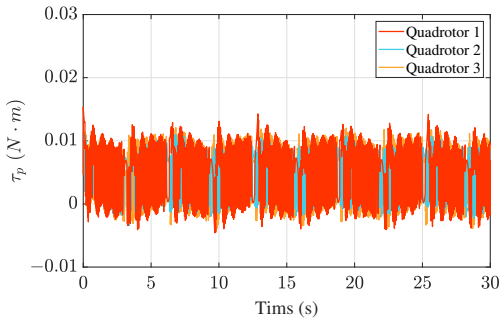
(**e**) Trajectory of ESO.



(**f**) Tracking error of ESO.

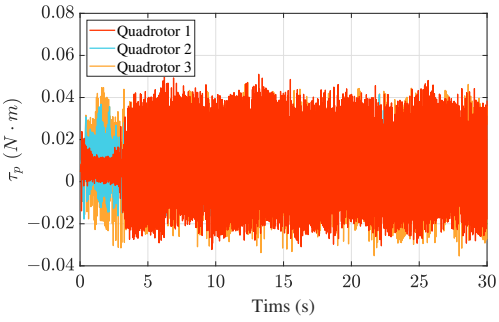


(**g**) τ_{ip} of MEE+UDE.

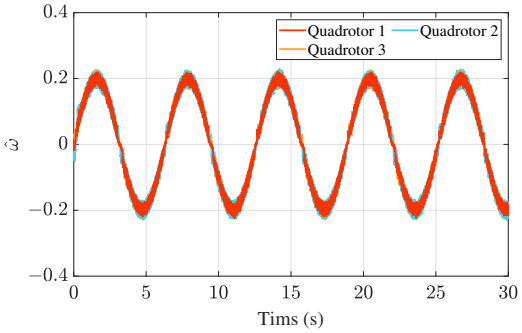


(**h**) τ_{ip} of RISE.

Figure 9. *Cont.*



(**i**) τ_{ip} of ESO.

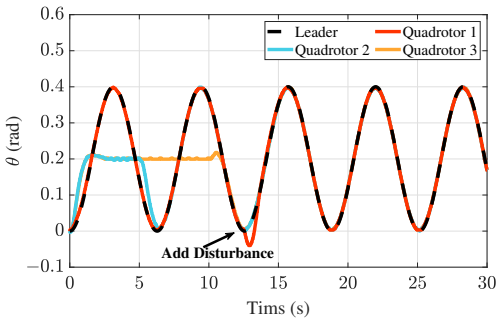


(**j**) Noise estimation generated by MEE.

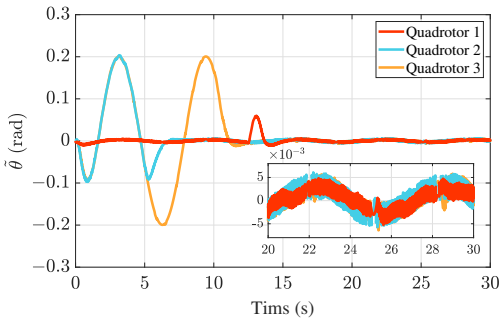
Figure 9. Experimental results of Case 1.

6.4. Case 2: Consensus Tracking Under Switching Communication and External Disturbance

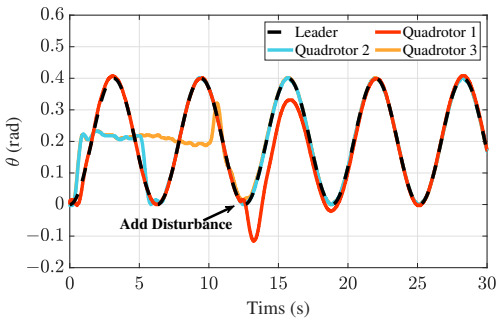
In this case, we consider the communication topology specified in Figure 8. In addition to the switching topology, a time-varying disturbance is manually introduced to quadrotor 1 by attaching a payload to the rotor safety guard while all three quadrotors are synchronized. This setup comprehensively verifies the advantages of the proposed framework in terms of both reference estimation and robust tracking control. Figure 10 shows the experimental results of Case 2. From the reference estimation perspective, quadrotor 1 can initially obtain the leader's states, while quadrotors 2 and 3 must estimate the leader's states in Stage 2 and Stage 3, respectively. From the robust tracking control perspective, the reference of quadrotors 2 and 3 is a step signal before they obtain the leader's states. The MEE+UDE-based controller performs the best transient and steady-state performance, outperforming the RISE-based controller, which is slower, while the ESO-based controller delivers obvious oscillations. After introducing the external disturbance, the MEE+UDE-based controller rapidly compensates for it. In contrast, the RISE-based controller compensates for the disturbance slowly, and the ESO-based controller gives a large torque command and shows worse steady-state performance (see 20 s–30 s). Figure 10j presents the noise estimation term generated by MEE.



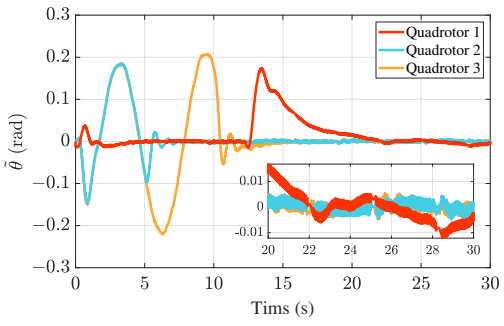
(**a**) Trajectory of MEE+UDE.



(**b**) Tracking error of MEE+UDE.

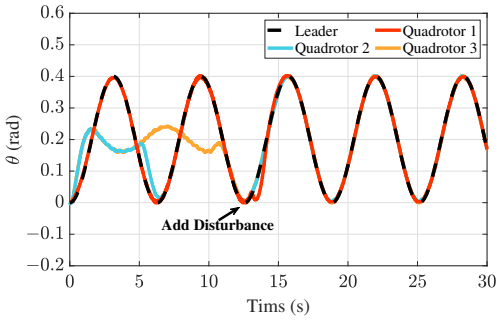


(**c**) Trajectory of RISE.

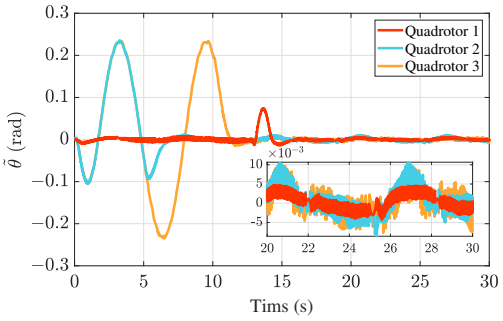


(**d**) Tracking error of RISE.

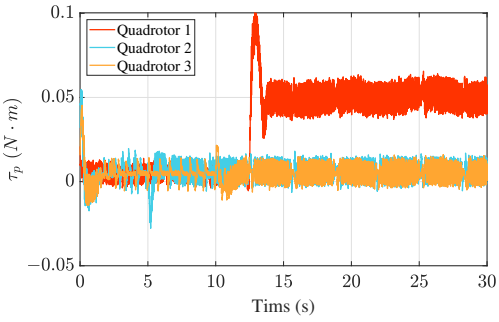
Figure 10. *Cont.*



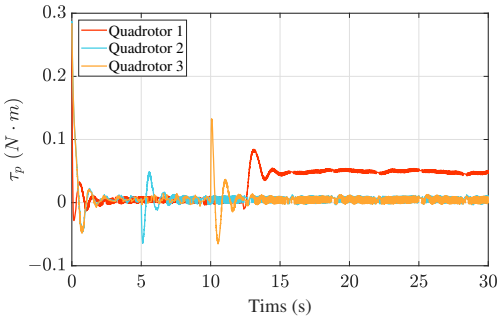
(**e**) Trajectory of ESO.



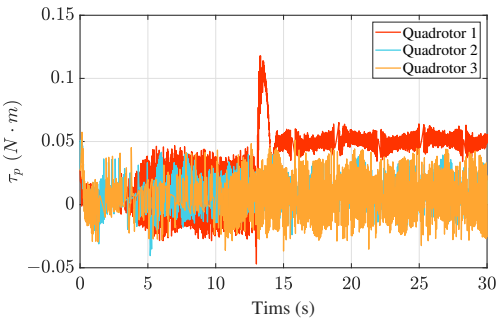
(**f**) Tracking error of ESO.



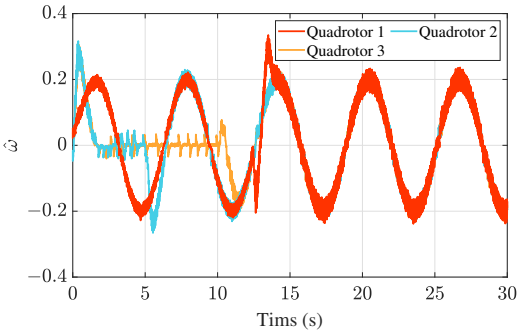
(**g**) τ_{ip} of MEE+UDE.



(**h**) τ_{ip} of RISE.



(**i**) τ_{ip} of ESO.

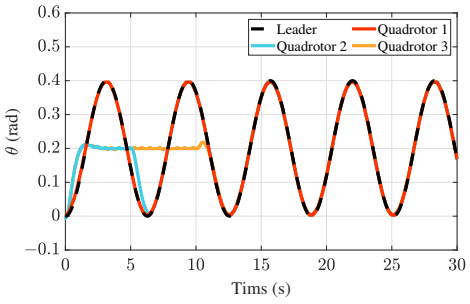


(**j**) Noise estimation generated by MEE.

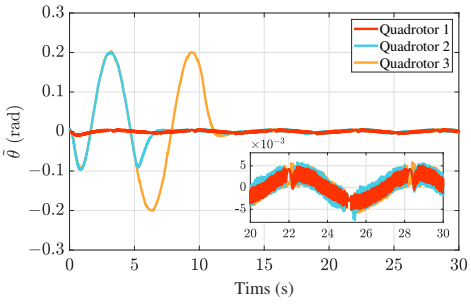
Figure 10. Experimental results of Case 2.

6.5. Case 3: Consensus Tracking Under Different Parameter ε

In this section, to verify Theorem 2, we apply different values of ε for the proposed MEE+UDE-based controller. We set $T_{id}^{*} = 0.1$, $T_{i\omega}^{*} = 0.1$ and choose ε values of 1, 10, and 100, respectively. Figure 11 depicts the experimental results. It is seen that as ε decreases, the tracking error can be reduced, which is consistent with Theorem 2.

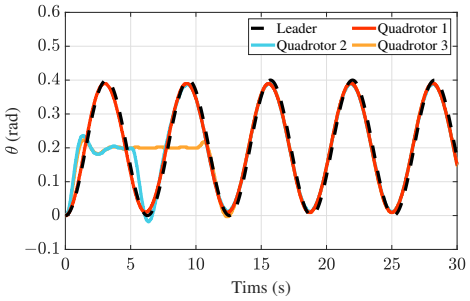


(**a**) Trajectory of $\varepsilon = 1$.

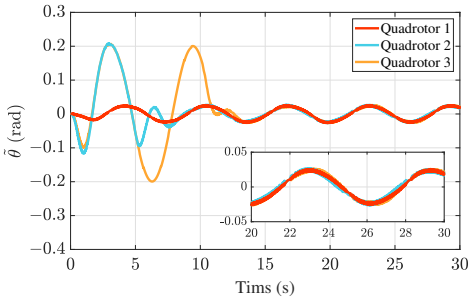


(**b**) Tracking error of $\varepsilon = 1$.

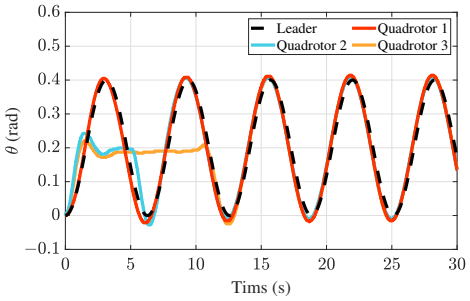
Figure 11. *Cont.*



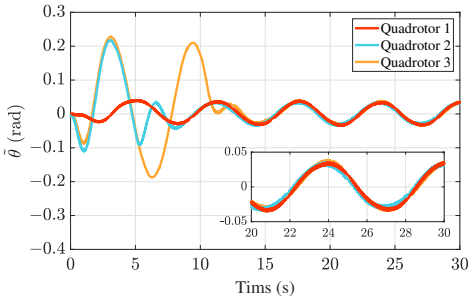
(**c**) Trajectory of $\varepsilon = 10$.



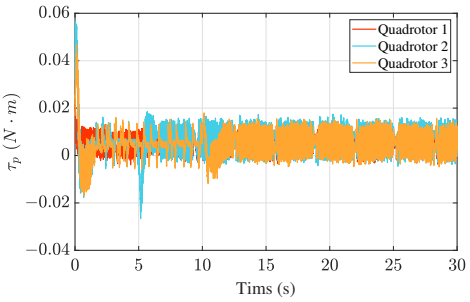
(**d**) Tracking error of $\varepsilon = 10$.



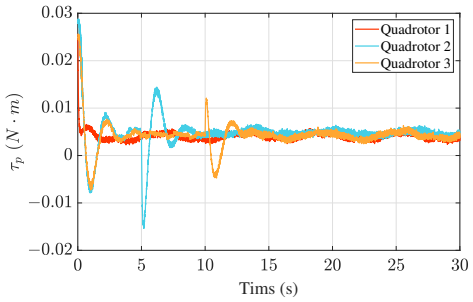
(**e**) Trajectory of $\varepsilon = 100$.



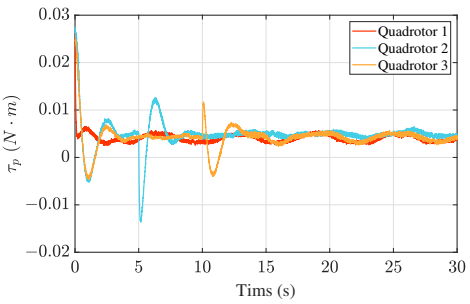
(**f**) Tracking error of $\varepsilon = 100$.



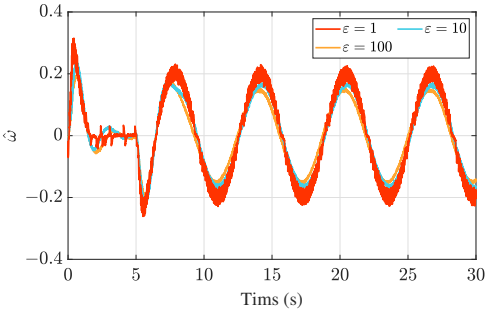
(**g**) τ_{ip} of $\varepsilon = 1$.



(**h**) τ_{ip} of $\varepsilon = 10$.



(**i**) τ_{ip} of $\varepsilon = 100$.



(**j**) Noise estimation generated by MEE.

Figure 11. Experimental results of Case 3.

7. Conclusions

In this paper, the consensus tracking problem for the multi-UAV systems with measurement noise and disturbance under switching communication topology has been investigated. To address this challenge, we have proposed a novel control framework comprising two distinct components: a distributed observer and a dual-estimator-based local tracking controller. The coupled design of MEE and UDE can mitigate the inherent drawback of the traditional UDE, which magnifies measurement noise. To simplify the tuning of MEE and UDE, parameter mapping has been conducted to relate the parameter ε with the MEE parameter $T_{i\omega}$ and UDE parameter T_{id}. The singular perturbation-theorem-based

analysis has revealed that reducing the single parameter ε can monotonically improve the system control performance. Finally, both the numerical simulation and experimental results verify the effectiveness of the proposed control framework. In the experiment in Case 2, the steady-state error of the proposed controller is 11.9% of RISE and 5.1% of ESO when tracking a step signal, and 50.4% of RISE and 57.2% of ESO when tracking a circular trajectory. In the experiment in Case 3, the steady-state tracking error decreased by 86.8% when tuning ε from 100 to 1.

The communication and input delays, which are commonly encountered in practice, have not been considered in this paper. In the future, we will further explore the consensus tracking and formation control of multi-UAV systems in the presence of communication delay, measurement noise, and external disturbances.

Author Contributions: Conceptualization, Z.Z., J.S. and Y.Z.; methodology, Z.Z., Y.Z. and E.W.; software, S.T.; validation, Z.Z., S.T. and Y.Z.; formal analysis, Z.Z. and E.W.; investigation, S.T. and E.W.; resources, Y.Z.; data curation, Z.Z.; writing—original draft preparation, Z.Z.; writing—review and editing, Z.Z., Y.Z. and J.S.; visualization, Z.Z. and S.T.; supervision, J.S. and Y.Z.; project administration, J.S. and Y.Z.; funding acquisition, J.S. and Y.Z. All authors have read and agreed to the published version of the manuscript.

Funding: This research was supported in part by the National Natural Science Foundation of China under Grant 62273077 and 62403397, the Natural Science Foundation of Sichuan Province 2024NSFJQ0013, and the New Cornerstone Science Foundation through the XPLORER PRIZE.

Institutional Review Board Statement: Not applicable.

Informed Consent Statement: Not applicable.

Data Availability Statement: Data are contained within the article.

DURC Statement: Current research is limited to the control theory, which is beneficial and does not pose a threat to public health or national security. Authors acknowledge the dual-use potential of the research involving control theory and confirm that all necessary precautions have been taken to prevent potential misuse. As an ethical responsibility, authors strictly adhere to relevant national and international laws about DURC. Authors advocate for responsible deployment, ethical considerations, regulatory compliance, and transparent reporting to mitigate misuse risks and foster beneficial outcomes.

Conflicts of Interest: The authors declare no conflicts of interest.

Abbreviations

The following abbreviations are used in this manuscript:

ESO	Extended state observer
ISS	Input-to-state stable
MEE	Measurement error estimator
RISE	Robust integral of the sign of the error
UAV	Unmanned aerial vehicles
UDE	Uncertainty and disturbance estimator

References

1. Amirkhani, A.; Barshooi, A.H. Consensus in Multi-Agent Systems: A Review. *Artif. Intell. Rev.* **2022**, *55*, 3897–3935. [CrossRef]
2. Patrinopoulou, N.; Daramouskas, I.; Meimetis, D.; Lappas, V.; Kostopoulos, V. A Multi-Agent System Using Decentralized Decision-Making Techniques for Area Surveillance and Intruder Monitoring. *Drones* **2022**, *6*, 357. [CrossRef]
3. Liu, Y.; Liu, J.; He, Z.; Li, Z.; Zhang, Q.; Ding, Z. A Survey of Multi-agent Systems on Distributed Formation Control. *Unmanned Syst.* **2024**, *12*, 913–926. [CrossRef]

4. Jin, X.; Hu, Z. Adaptive Cooperative Load Transportation by A Team of Quadrotors with Multiple Constraint Requirements. *IEEE Trans. Intell. Transp. Syst.* **2022**, *24*, 801–814. [CrossRef]
5. Wang, Y.; Yu, G.; Xie, W.; Zhang, W.; Silvestre, C. Robust Cooperative Transportation of a Cable-Suspended Payload by Multiple Quadrotors Featuring Cable-Reconfiguration Capabilities. *IEEE Trans. Intell. Transp. Syst.* **2024**, *25*, 11833–11843. [CrossRef]
6. Goodman, J.R.; Beckers, T.; Colombo, L.J. Geometric Control for Load Transportation with Quadrotor UAVs by Elastic Cables. *IEEE Trans. Control Syst. Technol.* **2023**, *31*, 2848–2862. [CrossRef]
7. Wan, P.; Xu, G.; Chen, J.; Zhou, Y. Deep Reinforcement Learning Enabled Multi-UAV Scheduling for Disaster Data Collection with Time-Varying Value. *IEEE Trans. Intell. Transp. Syst.* **2024**, *25*, 6691–6702. [CrossRef]
8. Zhou, Y.; Jin, Z.; Shi, H.; Shi, L.; Lu, N.; Dong, M. Enhanced Emergency Communication Services for Post-Disaster Rescue: Multi-IRS Assisted Air-Ground Integrated Data Collection. *IEEE Trans. Netw. Sci. Eng.* **2024**, *11*, 4651–4664. [CrossRef]
9. Zheng, J.; Ding, M.; Sun, L.; Liu, H. Distributed Stochastic Algorithm Based on Enhanced Genetic Algorithm for Path Planning of Multi-UAV Cooperative Area Search. *IEEE Trans. Intell. Transp. Syst.* **2023**, *24*, 8290–8303. [CrossRef]
10. Balanji, H.M.; Guven, I. Dynamic Multi-UAV Path Planning for Multi-Target Search and Connectivity. *IEEE Trans. Veh. Technol.* **2024**, *73*, 10516–10528.
11. Zhou, Y.; Wen, G.; Wan, Y.; Fu, J. Consensus Tracking Control for A Class of General Linear Hybrid Multi-Agent Systems: A Model-Free Approach. *Automatica* **2023**, *156*, 111198. [CrossRef]
12. Nan, X.; Lv, Y.; Duan, Z. Bipartite Consensus Tracking for Antagonistic Topologies with Leader's Unknown Input. *Asian J. Control* **2020**, *24*, 547–561. [CrossRef]
13. Aldana-López, R.; Gómez-Gutiérrez, D.; Defoort, M.; Sánchez-Torres, J.D.; Muñoz-Vázquez, A.J. A Class of Robust Consensus Algorithms with Predefined-Time Convergence under Switching Topologies. *Int. J. Robust Nonlinear Control* **2019**, *29*, 6179–6198. [CrossRef]
14. Gong, J.; Wang, F.; Liu, Z.; Chen, Z. Practical Fixed-Time Consensus Tracking for Second-Order Multi-Agent Systems with Mismatched Disturbances. *IEEE Trans. Signal Inf. Process. Over Netw.* **2023**, *9*, 761–769. [CrossRef]
15. Wang, X.; Xu, Y.; Cao, Y.; Li, S. A Hierarchical Design Framework for Distributed Control of Multi-Agent Systems. *Automatica* **2024**, *160*, 111402. [CrossRef]
16. Djaidja, S.; Wu, Q. An Overview of Distributed Consensus of Multi-Agent Systems with Measurement/Communication Noises. In Proceedings of the 2015 34th Chinese Control Conference (CCC), Hangzhou, China, 28–30 July 2015; pp. 7285–7290.
17. Zhou, R.; Feng, Y.; Di, B.; Zhao, J.; Hu, Y. Multi-UAV Cooperative Target Tracking with Bounded Noise for Connectivity Preservation. *Front. Inf. Technol. Electron. Eng.* **2020**, *21*, 1494–1503. [CrossRef]
18. Yan, D.; Zhang, W.; Chen, H.; Shi, J. Robust Control Strategy for Multi-UAVs System Using MPC Combined with Kalman-Consensus Filter and Disturbance Observer. *ISA Trans.* **2023**, *135*, 35–51. [CrossRef]
19. Hu, J.; Feng, G. Distributed Tracking Control of Leader–follower Multi-Agent Systems Under Noisy Measurement. *Automatica* **2010**, *46*, 1382–1387. [CrossRef]
20. Li, C.; Zong, X. Group Consensus of Multi-Agent Systems with Additive Noises. *Sci. China Inf. Sci.* **2022**, *65*, 202205. [CrossRef]
21. Zong, X.; Li, T.; Zhang, J.F. Consensus Conditions of Continuous-Time Multi-Agent Systems with Additive and Multiplicative Measurement Noises. *SIAM J. Control Optim.* **2018**, *56*, 19–52. [CrossRef]
22. Liu, Z.; Zhang, M.; Saberi, A.; Stoorvogel, A.A. Scale-Free Collaborative Protocol Design for Exact Output Synchronization of Multi-Agent Systems in the Presence of Disturbances and Measurement Noise with Known Frequencies. *IEEE Trans. Netw. Sci. Eng.* **2024**, *11*, 5720–5731. [CrossRef]
23. Huang, X.; Chen, Y.; Zhan, J. Observer-Based Consensus Control for Multi-Agent Systems with Measurement Noises and External Disturbances. *Int. J. Robust Nonlinear Control* **2020**, *32*, 344–357. [CrossRef]
24. Yang, G.; Rezaee, H.; Alessandri, A.; Parisini, T. State estimation using a network of distributed observers with switching communication topology. *Automatica* **2023**, *147*, 110690. [CrossRef]
25. Su, Y.; Huang, J. Cooperative Output Regulation with Application to Multi-Agent Consensus under Switching Network. *IEEE Trans. Syst. Man Cybern.–Part B Cybern.* **2012**, *42*, 864–875.
26. Bianchi, D.; Di Gennaro, S.; Di Ferdinando, M.; Acosta Lùa, C. Robust Control of UAV with Disturbances and Uncertainty Estimation. *Machines* **2023**, *11*, 352. [CrossRef]
27. Zhu, Y.; Zhu, B.; Liu, H.H.; Qin, K. Rejecting the Effects of Both Input Disturbance and Measurement Noise: A Second-Order Control System Example. *Int. J. Robust Nonlinear Control* **2020**, *30*, 6813–6837. [CrossRef]
28. Khalil, H.K.; Grizzle, J.W. *Nonlinear Systems*, 3rd ed.; Prentice-Hall: Upper Saddle River, NJ, USA, 2002.
29. Beard, R. *Quadrotor Dynamics and Control Rev 0.1*; Faculty Publications: Logan, UT, USA, 2008.
30. Stevens, B.L.; Lewis, F.L.; Johnson, E.N. *Aircraft Control and Simulation: Dynamics, Controls Design, and Autonomous Systems*, 3rd ed.; John Wiley and Sons, Inc.: New York, NY, USA, 2015.

31. Sankaranarayanan, V.N.; Satpute, S.; Nikolakopoulos, G. Adaptive Robust Control for Quadrotors with Unknown Time-Varying Delays and Uncertainties in Dynamics. *Drones* **2022**, *6*, 220. [CrossRef]
32. Quanser. Aero 2. Available online: https://www.quanser.com/products/aero-2 (accessed on 8 January 2025).

Disclaimer/Publisher's Note: The statements, opinions and data contained in all publications are solely those of the individual author(s) and contributor(s) and not of MDPI and/or the editor(s). MDPI and/or the editor(s) disclaim responsibility for any injury to people or property resulting from any ideas, methods, instructions or products referred to in the content.